Pergamon

0306-4522(95)00483-1

Neuroscience Vol. 71, No. 2, pp. 397–410, 1996
Elsevier Science Ltd
IBRO
Printed in Great Britain

MODELING *N*-METHYL-D-ASPARTATE-INDUCED BURSTING IN DOPAMINE NEURONS

Y.-X. LI,* R. BERTRAM and J. RINZEL

Mathematical Research Branch, National Institute of Diabetes and Digestive and Kidney Diseases, National Institutes of Health, Bethesda, MD 20892, U.S.A.

Abstract—Burst firing of dopaminergic neurons of the substantia nigra pars compacta can be induced *in vitro* by the glutamate agonist *N*-methyl-D-aspartate. It has been suggested that the interburst hyperpolarization is due to Na^+ extrusion by a ouabain-sensitive pump [Johnson *et al.* (1992) *Science* **258,** 665–667]. We formulate and explore a theoretical model, with a minimal number of currents, for this novel mechanism of burst generation. This minimal model is further developed into a more elaborate model based on observations of additional currents and hypotheses about their spatial distribution in dopaminergic neurons [Hounsgaard (1992) *Neuroscience* **50,** 513–518; Llinás *et al.* (1984) *Brain Res.* **294,** 127–132]. Using the minimal model, we confirm that interaction between the regenerative, inward *N*-methyl-D-aspartate-mediated current and the outward Na^+-pump current is sufficient to generate the slow oscillation ($\sim$0.5 Hz) underlying the burst. The negative-slope region of the *N*-methyl-D-aspartate channel's current–voltage relation is indispensable for this slow rhythm generation. The time-scale of Na^+-handling determines the burst's slow frequency. Moreover, we show that, given the constraints of sodium handling, such bursting is best explained mechanistically by using at least two spatial, cable-like compartments: a soma where action potentials are produced and a dendritic compartment where the slow rhythm is generated. Our result is consistent with recent experimental evidence that burst generation originates in distal dendrites [Seutin *et al.* (1994) *Neuroscience* **58,** 201–206]. Responses of the model to a number of electrophysiological and pharmacological stimuli are consistent with known responses observed under similar conditions. These include the persistence of the slow rhythm when the tetrodotoxin-sensitive Na^+ channel is blocked and when the soma is voltage-clamped at -60 mV. Using our more elaborate model, we account for details of the observed frequency adaptation in *N*-methyl-D-aspartate-induced bursting, the origin of multiple spiking and bursting mechanisms, and the interaction between two different bursting mechanisms. Besides reproducing several well established firing patterns, this model also suggests that new firing modes, not yet recorded, might also occur in dopaminergic neurons.

This model provides mechanistic insights and explanations into the origin of a variety of experimentally observed membrane potential firing patterns in dopaminergic neurons, including *N*-methyl-D-aspartate-induced bursting and its dendritic origin. Such a model, capable of reproducing a number of realistic behaviors of dopaminergic neurons, could be useful in further studies of the basal ganglia-thalamocortical motor circuit. It may also shed light on bursting that involves *N*-methyl-D-aspartate channel activity in other neuron types.

Key words: basal ganglia, glutamate agonist, sodium pump, oscillations, firing patterns.

Dopaminergic (DA) neurons of the substantia nigra pars compacta have been shown to exhibit two major patterns of membrane potential discharge *in vivo*: slow single spike firing of 3–8 Hz and burst firing of fast spikes of 10–20 Hz with interburst intervals longer than 1 s.[14,15] While there is substantial evidence suggesting that the spontaneous single spike firing is generated endogenously in DA neurons,[5,18] the mechanism for burst generation *in vivo* remains unclear. Recent studies[26,40,41,42] of bursting in slice preparations have provided new evidence and hypotheses for burst rhythmogenesis in DA neurons. These experiments illustrate that, unlike several other cell types in which the apamin-sensitive Ca^{2+}-activated potassium current [$I_{K(Ca)}$] plays a role in burst generation,[17,24,29,44] DA neurons more readily exhibit bursting in the absence of $I_{K(Ca)}$. Of particular interest is the compelling evidence, reported by Johnson and coworkers (1992), showing that robust bursting occurred in slice preparations when the glutamate agonist *N*-methyl-D-aspartate (NMDA) was applied to the bath.[26] This suggests that perhaps critical afferent glutamatergic inputs, lost in slice preparations, play an important role in burst-generation in DA neurons. Furthermore, their experiments indicate that Na^+-influx through NMDA receptor channels activates the ouabain-sensitive Na^+ pump, and the outward pump current is responsible for the interburst hyperpolarization in DA neurons.

*To whom correspondence should be addressed at: MRB, NIDDK, NIH, 9190 Wisconsin Ave, Suite 350, Bethesda, MD 20814, U.S.A.

Abbreviations: DA, dopaminergic; NMDA, *N*-methyl-D-aspartate; TEA, tetraethylammonium; TTX, tetrodotoxin.

To test the viability of this novel burst-generating mechanism, we formulate and explore a theoretical model of DA neurons that incorporates the NMDA channel and the Na^+ pump. Our model reproduces several characteristic firing patterns including spontaneous repetitive spiking and NMDA-mediated bursting in DA neurons. We also develop a more detailed version of the model by incorporating other currents known to exist in these neurons. Besides producing more realistic profiles of NMDA-induced bursting, this more elaborate model enables us to explore multiple spiking and bursting mechanisms in DA neurons. An abstract of this work has appeared.[30]

MODEL AND NUMERICAL METHODS

As found valuable in other recent studies,[3,7,34] we employ a model that crudely approximates neuronal cable properties with only two compartments: a soma compartment that also includes the proximal dendrites, and a dendritic compartment that represents the distal dendrites, lumped together (see Fig. 1). The two compartments are coupled electrotonically with a coupling conductance, $A_T g_c$, where A_T is the total surface area of the neuron and, for notational convenience, we have expressed g_c as a density. The coupling current that flows between the two compartments is $\pm A_T g_c(V_D - V_S)$. Thus coupling current terms in the current balance equations (per unit area) of the soma and the dendrite are

$$\frac{g_c}{p}(V_D - V_S) \quad \text{and} \quad \frac{g_c}{1-p}(V_S - V_D),$$

respectively. Here, p and $1-p$ are, respectively, the ratios of the soma area and the dendrite area to the total area A_T; the subscript S denotes soma and D denotes dendrite. A direct derivation of the values of g_c and p (see Table 1 in the Appendix) from a detailed continuous cable model with a branched dendritic architecture has not yet been developed.[34] Instead, we use empirical estimates for these parameters to yield reasonable attenuation and firing characteristics.

The ionic basis for the voltage firing of DA neurons *in vitro* has been studied extensively[14–16,28,31,33] and a rich variety of current types have been characterized. These include the tetrodotoxin (TTX)-sensitive Na^+ current, two types of Ca^{2+} currents (the L-type and the T-type), three types of K^+ currents (the delayed-rectifier, the apamin-sensitive Ca^{2+}-dependent SK type and the delayed-repolarizing A-type), and an anomalous rectifier (sag) current. We incorporate these currents in our detailed version of the model (see Appendix) according to a previously proposed[31] scheme of current distribution in DA neurons. To focus on the NMDA-mediated bursting, however, we first study a reduced model containing the minimal number of currents sufficient to illustrate the underlying mechanism. Based on recent observations,[41] we assume that the fast spiking is generated in the soma and the slow rhythm of recurrent hyperpolarization is generated in the dendrite. Minimal descriptions of these two compartments are presented in the following sections.

Soma compartment

The fast spiking in NMDA-induced burst firing is sensitive to TTX and persists in Ca^{2+}-deficient medium.[26] Therefore, we only consider the TTX-sensitive Na^+ channel and the delayed-rectifier K^+ channel in our minimal description of this Na^+ spiking. We use a Hodgkin–Huxley-type formulation[21] to describe the corresponding currents:

$$I_{Na} = g_{Na} m_\infty^3 h(V_S - V_{Na}) \text{ and}$$

$$I_{K-DR} = g_{K-DR} n^2 (V_S - V_K).$$

Here, we use n^2 in the expression for I_{K-DR}, although other powers of n could be used provided that action potentials are generated. We assume that activation of the Na^+ channel is instantaneous. Equations governing the time dependent behaviour of V_S and the gating variables (h, n) are:

$$C_m \frac{dV_S}{dt} = -I_{K-DR} - I_{Na} - \frac{g_c}{p}(V_S - V_D),$$

$$\frac{dh}{dt} = [h_\infty(V_S) - h]/\tau_h(V_S),$$

$$\frac{dn}{dt} = [n_\infty(V_S - n]/\tau_n(V_S), \qquad \text{(Eqn 1)}$$

where C_m is the membrane capacitance per unit area. Definitions of the gating functions h_∞, τ_h, n_∞, τ_n, and the parameter values are given in the Appendix. For simplicity, no particular pacemaker current is introduced into the soma model. Therefore, the soma compartment is quiescent ($V_S = -64$ mV) when decoupled from the dendritic compartment (i.e. when $g_c = 0$). Tonic spiking is possible only when the two compartments are coupled and when the dendrite (whose resting potential is less negative than the soma's) exerts a small but steady depolarizing

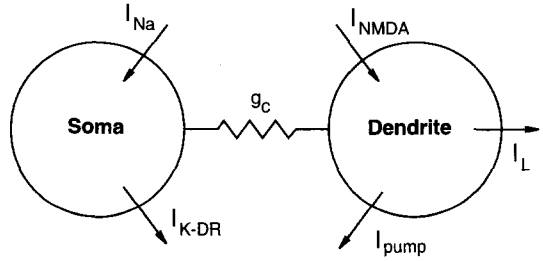

Fig. 1. Schematic representation of the minimal model of a DA neuron. It consists of a spike-producing compartment (soma) and a slow rhythm-generating compartment (lumped dendrite). The two compartments are electrotonically coupled with coupling conductance g_c. The types of ionic channels considered are just sufficient for a qualitative understanding of the mechanism underlying NMDA-induced bursting in DA neurons. No voltage-dependent channels other than the NMDA channel are considered in the dendrite in this minimal model.

influence on the soma. The existence of a slowly depolarizing pacemaker current has been reported,[16] but no particular channel was identified as the carrier of the current. Besides, the sag current I_h, which will be included in the more detailed model, can also act as a pacemaker.[16]

Dendritic compartment

We model the dendritic compartment in a way that emphasizes its ability to generate the slow rhythm underlying the NMDA-induced burst firing. This slow rhythm is determined by two crucial elements, the NMDA receptor channel and the Na^+ pump. It is insensitive to TTX, apamin, and to changes in both extra- and intracellular Ca^{2+} concentrations.[26,40] We therefore study a minimal dendritic model consisting of the NMDA current (I_{NMDA}), the electrogenic Na^+ pump current (I_{pump}), and a leak current (I_L). Na^+ concentration in the dendrite (Na) is an important dynamic variable since it controls the rate of Na^+-extrusion by the pump. The equations describing the time-dependent evolution of V_D and Na are given as follows:

$$C_m \frac{dV_D}{dt} = -I_{NMDA} - I_{pump} - I_L - \frac{g_c}{1-p}(V_D - V_S),$$

$$\frac{dNa}{dt} = \alpha[-I_{Na,NMDA} - 3I_{pump}]. \quad \text{(Eqn 2)}$$

The leak current is defined as $I_L = g_L(V_D - V_L)$. The parameter α, which converts Na^+ current into Na^+ flux, is defined as the inverse of the product of Faraday's constant F and the volume–area ratio; for a locally cylindrical dendrite branch of radius r_D, $\alpha = 1/(0.5 r_D F)$. The Na^+ pump is known to exchange 3 Na^+ ions (outward) for 2 K^+ ions (inward) by consuming one ATP molecule. We assume that Na^+-exchange between the soma and the dendrite through diffusion is weak; we neglect it in our model so that Na^+ concentrations in the two compartments are independent. In this minimal description, Na^+ concentration in the soma is fixed.

Besides the ATP concentration, the pump activity generally depends on Na, extracellular Na^+ and K^+ concentrations ($[Na^+]_e$, $[K^+]_e$), and the membrane voltage.[8] The values of $[K^+]_e$ and $[Na^+]_e$ are fixed in our study. The voltage sensitivity is weak for membrane voltages ranging from -100 up to 150 mV[19] and is thus ignored. Therefore, Na becomes the only factor controlling the pump activity. This yields a simplified description of the pump current:

$$I_{pump}(Na) = R_{pump}[\phi(Na) - \phi(Na_{eq})], \quad \text{(Eqn 3)}$$

where R_{pump} is the maximum pump current, and Na_{eq} is the value of Na at which the pump current vanishes. We assume that the pump rate changes instantaneously as a function of Na, and that $\phi(Na) = Na^3/(Na^3 + K_p^3)$. The cubic nonlinearity is related to the cooperative binding of 3 Na^+ ions to the pump molecule in the early steps of Na^+ transport. The current defined in Eqn 3 is the difference between the actual pump current $R_{pump}\phi(Na)$ and a constant inward Na^+ leak current into the dendrite, $R_{pump}\phi(Na_{eq})$. We use this expression for the constant inward Na^+ leak current to emphasize that the pump is able to balance the leak when $Na = Na_{eq}$.

Voltage-sensitivity of the NMDA channel conductance in the presence of Mg^{2+} is essential in generating the slow rhythm.[26] Voltage-clamp experiments have revealed the mechanism of the NMDA channel's voltage-sensitivity[32] and determined the voltage-sensitivity of the kinetic constants of Mg^{2+} block.[1] Kinetic models of the channel's gating properties have been developed,[25,22] all yielding an expression similar to the following one that we use for the NMDA current I_{NMDA} in our dendritic model.

$$I_{NMDA} = \left[\frac{g_{NMDA}}{1 + \frac{[Mg^{2+}]_o}{K_{Mg}}\exp\left(-\frac{V_D}{q}\right)}\right](V_D - V_{NMDA}), \quad \text{(Eqn 4)}$$

where $[Mg^{2+}]_o$ denotes the extracellular Mg^{2+} concentration, and $V_{NMDA} = 0$. I_{NMDA} is a combination of at least three different currents: $I_{Na,NMDA}$, $I_{Ca,NMDA}$ which are inward, and the outward $I_{K,NMDA}$.

For simplicity, we assume that $I_{Na,NMDA}$ inherits the same voltage-sensitivity as I_{NMDA} but maintains its own reversal potential V_{Na} and accounts for a fraction of the overall conductance g_{NMDA}. Therefore,

$$I_{Na,NMDA} = \left[\frac{g_{Na,NMDA}}{1 + \frac{[Mg^{2+}]_o}{K_{Mg}}\exp\left(\frac{-V_D}{q}\right)}\right](V_D - V_{Na})$$

In Eqn 4, the binding and unbinding of Mg^{2+} to the NMDA channel were treated as instantaneous since the kinetic rates associated with Mg^{2+} block are fast under normal physiological conditions.[1,25] The dynamic features of the dendritic compartment will be studied in detail in the following section.

Numerical methods

Gear's algorithm implemented in the LSODE package[20] was used in numerical integration of the ordinary differential equations. The tolerances were RTOL = ATOL = 10^{-9}.

RESULTS

N-*Methyl*-D-*aspartate-induced bursting in the minimal model*

Mechanism for the slow rhythm in the isolated dendrite. When the coupling conductance g_c is set to zero, the dendrite becomes an isolated compartment described by Eqn 2. In the absence of NMDA (i.e. when $g_{NMDA} = g_{Na,NMDA} = 0$), the dendrite has a stable (globally attracting) steady-state $V_D = V_L = -50$ mV, $Na = Na_{eq}$. When sufficient NMDA is present,

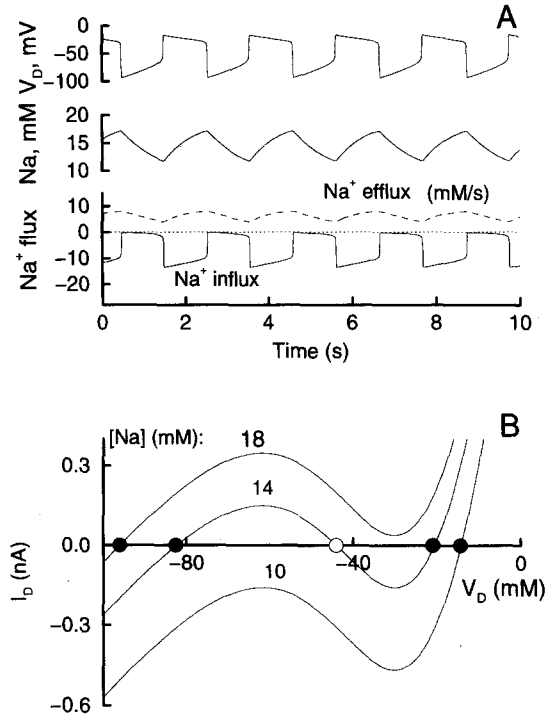

Fig. 2. Mechanism for slow rhythm generation in the dendritic compartment isolated from the soma. (A) NMDA-induced slow oscillations in the dendritic membrane potential V_D (top panel), in dendritic Na^+ concentration *Na* (middle panel), and in both inward and outward Na^+ fluxes (bottom panel). The thin dotted line in the bottom panel indicates zero flux. The influx is negative and the efflux positive. (B) The steady-state current–voltage curves for *Na* fixed at three different values. The crossing points of these curves with the zero-current axis correspond to the steady-states of the isolated dendrite at fixed *Na* values. The stable steady states are marked by a filled circle, the unstable one marked by an open circle. The rhythm arises as a consequence of the coexistence of two stable steady states over a range of *Na*-values and the transition between these states as the slowly varying *Na* reaches critical levels (see text). No spiking is seen since other active channels such as Na^+ and Ca^{2+} channels are ignored in this minimal dendritic compartment.

repetitive oscillations arise with a period of about 2 s (Fig. 2A). V_D oscillates in a squarewave profile (Fig. 2A, top panel), alternating between a depolarized level and a hyperpolarized level. During the depolarized phase, *Na* slowly accumulates (Fig. 2A, middle panel) and this accumulation increases Na^+ efflux by the pump (Fig. 2A, bottom panel). The growing outward current slowly repolarizes the dendrite causing a simultaneous decline in Na^+ influx through NMDA channels (Fig. 2A, bottom panel). When the sum of the outward pump current and the leak current (not shown) surpasses the inward current through NMDA channels, V_D rapidly hyperpolarizes and shuts down the NMDA current. During the hyperpolarized phase, Na^+ influx through NMDA channels is almost zero (Fig. 2A, bottom panel), and Na^+ concentration is slowly restored to a low level by the unopposed pump activity. During this phase, V_D slowly depolarizes. When *Na* is low enough, V_D reaches threshold for reactivating the NMDA current; rapid depolarization occurs and the cycle restarts.

An alternative description of the genesis of these oscillations is presented in Fig. 2B, where steady-state $I_D - V_D$ curves are plotted at three fixed values of *Na*. Here, the dendritic current I_D is defined as $I_D(V_D) = I_{NMDA}(V_D) + I_{pump}(Na) + I_L(V_D)$. This treatment of *Na* as a parameter is meaningful since it varies with a much slower time-scale than V_D. The negative slope in each N-shaped curve in Fig. 2B is directly linked to the negative resistance in the *I–V* relation of the NMDA current.[32] The crossing points of the $I_D - V_D$ curve with the zero-current axis, marked by a filled or an open circle, correspond to the steady-states of the isolated dendritic compartment at fixed *Na* levels. The filled circle denotes a stable steady-state, while the open circle refers to an unstable one. When *Na* is low, the $I_D - V_D$ curve (the bottom one in Fig. 2B) crosses the zero-current axis at a high value of V_D. Thus, the system stays in a depolarized state determined by the open NMDA channels. The resulting Na^+ influx increases *Na* slowly, and the $I_D - V_D$ curve slowly drifts upward. At a higher *Na* value, the $I_D - V_D$ curve (the middle one in Fig. 2B) crosses the horizontal axis three times creating two additional steady-states: the middle one is unstable (corresponding to a threshold voltage) while the leftmost one is stable. However, unless a substantial perturbation is applied to the system, it remains at the depolarized steady-state. When *Na* becomes sufficiently large, the $I_D - V_D$ curve intersects the horizontal axis only at a hyperpolarized voltage (top curve in Fig. 2B) and V_D rapidly drops to this steady value. The NMDA channels are closed now and the pumps are working at high capacity since *Na* has been elevated substantially. This leads to a slow decrease in *Na* which moves the $I_D - V_D$ curve downward again. As *Na* continues to decrease, the $I_D - V_D$ curve moves back below the horizontal axis and V_D jumps from the hyperpolarized level back to the depolarized level, restarting the cycle.

Results shown in Fig. 2 demonstrate that the interaction between the NMDA current I_{NMDA} and the pump current I_{pump} can generate the slow rhythm which may underlie NMDA-induced bursting. The negative slope in the *I–V* relation of the NMDA channel is the crucial regenerative mechanism. The slow time-scale in the alternation between the depolarized and the hyperpolarized state is determined by the slow time scale of Na^+-handling (accumulation and extrusion) in the dendritic compartment.

N-Methyl-D-aspartate turns tonic spiking into rhythmic bursting. Our model of a DA neuron, in its minimal form, is described by Eqns 1 and 2 with nonzero g_c. In the absence of NMDA the less polarized dendritic compartment exerts a depolarizing influence on the soma compartment. The associated coupling current flowing to the soma thus plays the

role of a pacemaker current in our minimal model. This causes tonic firing of regularly spaced action potentials in the soma which passively propagate to the dendrite with significant attenuation (Fig. 3A). The spiking frequency is about 5 Hz, which is within the frequency range (1–8 Hz) observed in DA neurons in slice preparation and in the absence of NMDA.[26]

In the continuous presence of NMDA, the tonic firing pattern is transformed into a bursting pattern, with bursts of fast spikes separated by interburst hyperpolarizations (Fig. 3B). This NMDA-induced bursting pattern possesses the physiological long period (~ 2 s) and agrees qualitatively with the experimentally observed pattern.[26] However, there exist obvious discrepancies between the model simulations and experimental records. The calculated spiking frequency (~ 100 Hz) during the plateau phase is much higher than observed frequencies (10–20 Hz). In addition, the computed interburst hyperpolarization (V_S reaches -90 mV) exceeds the observed levels (V_S reaches -70 to -80 mV). These discrepancies can be attributed to the omission of several currents from the minimal model. Both the sag current I_h and the low-threshold Ca^{2+} current I_{Ca-T} can reduce the magnitude of hyperpolarization, while the delayed repolarizing current I_A and the Ca^{2+}-dependent K^+ current $I_{K(Ca)}$ can reduce the spiking frequency during the plateau phase. Below, we will consider the effects of these other channels in more detail.

Blocking the fast spiking mechanism leaves the slow rhythm intact. Johnson and colleagues[26] showed that the slow rhythm underlying the NMDA-induced bursting persisted when TTX was applied. In more recent experiments,[41] slow oscillations in current were measured when the soma was voltage-clamped at -60 mV. These results support their hypothesis that the slow rhythm is generated distally at dendritic sites, not resulting solely from somatic activity. In our minimal model, the fast action potential spiking and the slow hyperpolarizing rhythm are generated separately in the soma and the dendrite. The TTX-sensitive Na^+ channel is not directly involved in the slow rhythm generation. However, when this inward current is eliminated, the unopposed K^+ current tends to polarize the soma, which in turn gives hyperpolarizing influence on the dendrite. Similar hyperpolarizing effects on the dendritic compartment exist when the soma is voltage-clamped at -60 mV. Therefore, the slow rhythm generating mechanism should be strong enough to resist substantial hyperpolarizing influence from the soma.

Indeed, the NMDA-induced rhythmicity in the model survives under these pharmacological and electrophysiological conditions. As shown in Fig. 4A, eliminating the TTX-sensitive Na^+ channel abolishes the fast soma spiking, but the slow rhythm persists, with a slightly increased period. Furthermore, when the soma voltage is clamped at -60 mV, the applied current I_{APP} required to hold it at this potential oscillates (Fig. 4B). The oscillation period is reduced threefold as compared to the bursting period in Fig. 3B. However, if the soma is clamped at a more negative voltage of -70 mV or lower, the dendritic rhythm disappears (not shown). This result is consistent with the experiments by Seutin and colleagues[40] who showed that oscillations disappear when the soma is voltage-clamped at about -80 mV with hyperpolarizing current-injections.

Na^+ pump inhibitors eliminate the repetitive hyperpolarization and convert bursting into continuous spiking. Important evidence supporting the role of the Na^+ pump in producing the burst firing pattern in NMDA-stimulated DA neurons was obtained using pump inhibitors.[26] These experiments showed that pharmacological manipulations that paralyse the pump activity consistently eliminated burst firing and, in the presence of TTX, eliminated slow voltage oscillations induced by NMDA. In particular, the pump inhibitor strophanthidin reversibly turned bursting into continuous spiking. (The continuous spiking seen with pump inhibitors and NMDA cannot last forever and the neuron eventually dies as a result of the continuous accumulation of Na^+ in the cell.) Our model is consistent with these results, as illustrated in Fig. 5 where the NMDA-induced bursting pattern is transformed into tonic spiking upon simulated blockage of the pump current.

N-Methyl-D-aspartate-induced burst firing is eliminated in Mg^{2+}-free medium. It has been found that a physiological concentration of extracellular Mg^{2+} is indispensable for burst firing in DA neurons.[26] The model simulation yields the same result. Applying NMDA to the model DA neuron in a Mg^{2+}-free medium (i.e. $[Mg^{2+}]_o = 0$ in Eqn 4) results in high frequency continuous spiking (not shown). The removal of the voltage-sensitive Mg^{2+}-block of the NMDA channel eliminates the negative slope in the membrane's $I_D - V_D$ relation.

Effects of other currents in a more elaborate model

In the minimal model we ignored several currents that are known to exist in DA neurons. These include I_{Ca-T}, I_{Ca-L}, I_A, $I_{K(Ca)}$ (apamin-sensitive), and I_h (anomalous rectifier or sag current).[14–16,28,31,33] To consider the effects of these currents on firing patterns, we follow the suggestion of Llinás and co-workers[31] with regard to where these currents are located with significant densities. We put I_{Ca-L} in the dendritic compartment and the others in the soma compartment. We also include the fast-activating and slow-inactivating I_A[28] in the soma. A delayed rectifier potassium current, I_{K-DR}, with moderate conductance is introduced in the dendritic compartment as a crude approximation to the polarizing currents that may exist in the distal dendrites. Equations describing this more elaborate model are given in the Appendix. We do not attempt an exhaustive description of the many possible dynamic behaviors for different

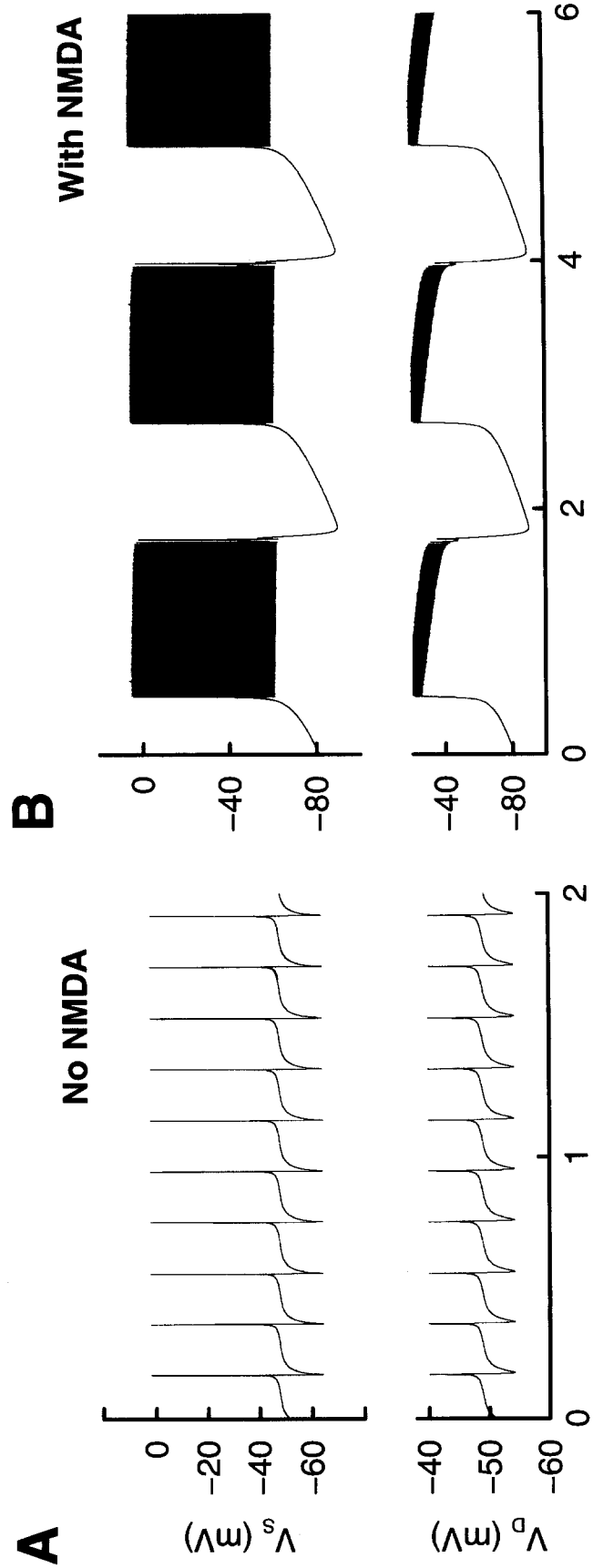

Fig. 3. Firing patterns of the minimal model in the absence (A) and in the presence (B) of NMDA. (A) Tonic firing of single spikes in the soma (top panel) and the dendrite (bottom panel) when coupled and without NMDA stimulation. The spiking frequency is about 5 Hz. (B) NMDA turns tonic spiking into a burst firing pattern with fast spiking (~100 Hz) on a depolarized plateau, separated by interburst hyperpolarizations. The bursting period is close to 0.5 Hz.

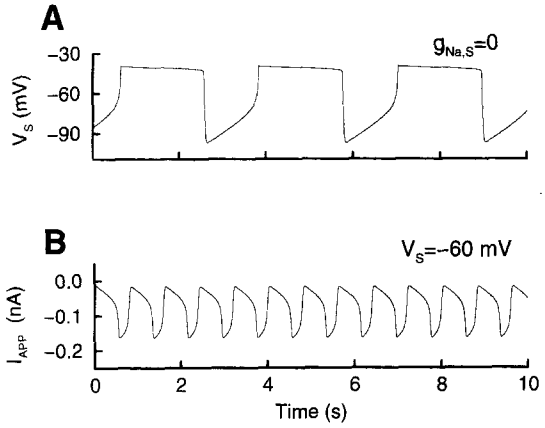

Fig. 4. The slow rhythm persists in the model when the fast spiking is eliminated by TTX (A) or by voltage-clamping the soma at −60 mV (B). However, the slow rhythm can be eliminated by clamping the soma at more negative voltages (not shown).

parameter values of this complex model. Instead, we illustrate several important effects of these newly incorporated currents.

$I_{K(Ca)}$ *and* I_A *contribute to frequency-adaptation during the burst phase.* Computations of the more elaborate model demonstrate that, for a range of magnitudes of the above mentioned currents, NMDA is still able to switch the model neuron's firing mode from tonic spiking to bursting (Fig. 6A). As compared to the minimal model (Fig. 3B), the bursting profile generated by this detailed model (Fig. 6) bears closer resemblance to experimental observations[26] in the following two aspects. First, the spiking frequency during each burst is now closer to the observed frequency.[26] This is mostly due to the additional hyperpolarizing effects of the newly added $I_{K(Ca)}$ and I_A, which both act to suppress the excessive depolarizing influence from the dendritic compartment when NMDA channels are constantly activated. Second, the progressive decline of the spiking frequency is better illustrated (see the enlarged profile in the right panel of each row). This gradual decrease of spiking frequency, often called frequency-adaptation, appears to be a characteristic feature of burst firing in DA neurons.[26,42]

Frequency-adaptation can be caused by a number of mechanisms. The two newly added K^+ currents in the soma compartment, $I_{K(Ca)}$ and I_A, both contribute to the occurrence of frequency-adaptation (Fig. 6B, C). Moreover, the gradual decline of the dendritic voltage V_D caused by the progressive increase in the Na^+ pump current during the dendritic plateau phase (see Fig. 2A) also contributes. This decreasing V_D-mediated frequency-adaptation mechanism also exists in the minimal model, but its effect there is negligible since the soma is over-depolarized during the plateau phase. When this excessive depolarization is counteracted by a hyperpolarizing current injection, frequency-adaptation can also be seen in the minimal model (not shown).

Figure 6B shows the best established effect of $I_{K(Ca)}$ in frequency-adaptation. $I_{K(Ca)}$ gradually increases during a burst as Ca^{2+} enters through voltage-gated Ca^{2+} channels and accumulates in the soma. This increasing $I_{K(Ca)}$ decreases the spiking frequency gradually. Figure 6C shows that frequency-reduction can happen in a different manner, occurring suddenly in the middle of a burst. When all frequency-adaptation generating mechanisms are present but with moderate strength (as in Fig. 6A), it is hard to determine which exerts the dominant effect. However, if any or all such currents are present with large strength, spiking may stop before the plateau phase terminates (not shown).

Multiple spike and burst generating mechanisms in the absence of N-*methyl*-D-*aspartate.* Dopaminergic neurons have been shown to possess multiple mechanisms for generating action potentials.[16,23,28] Interactions of the multiple channel types in our detailed model indeed create new spiking and bursting patterns in addition to those produced by the minimal model. These additional mechanisms are not related

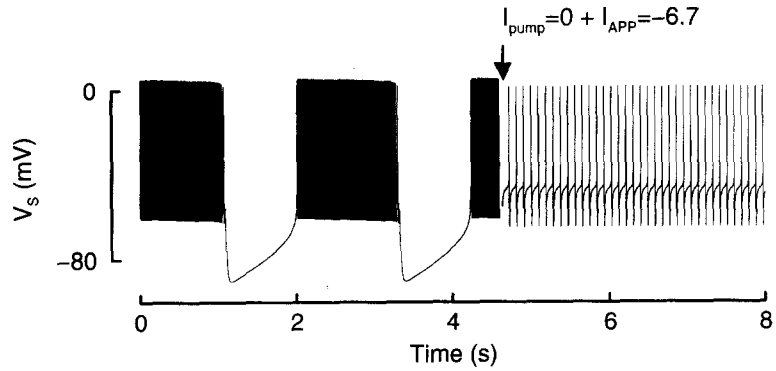

Fig. 5. Na^+ pump inhibitors transform the NMDA-induced bursting pattern into a tonic spiking pattern in model simulations. Notice that when the pump current is blocked, a hyperpolarizing current ($I_{APP} = -6.7\,\mu A/cm^2$) is applied that greatly reduces the tonic spiking frequency. Such an arrangement resembles the conditions of a similar experiment by Johnson and colleagues.[26] Stronger hyperpolarizing current injections or similar injections applied during the quiescent phase can abolish the oscillations.

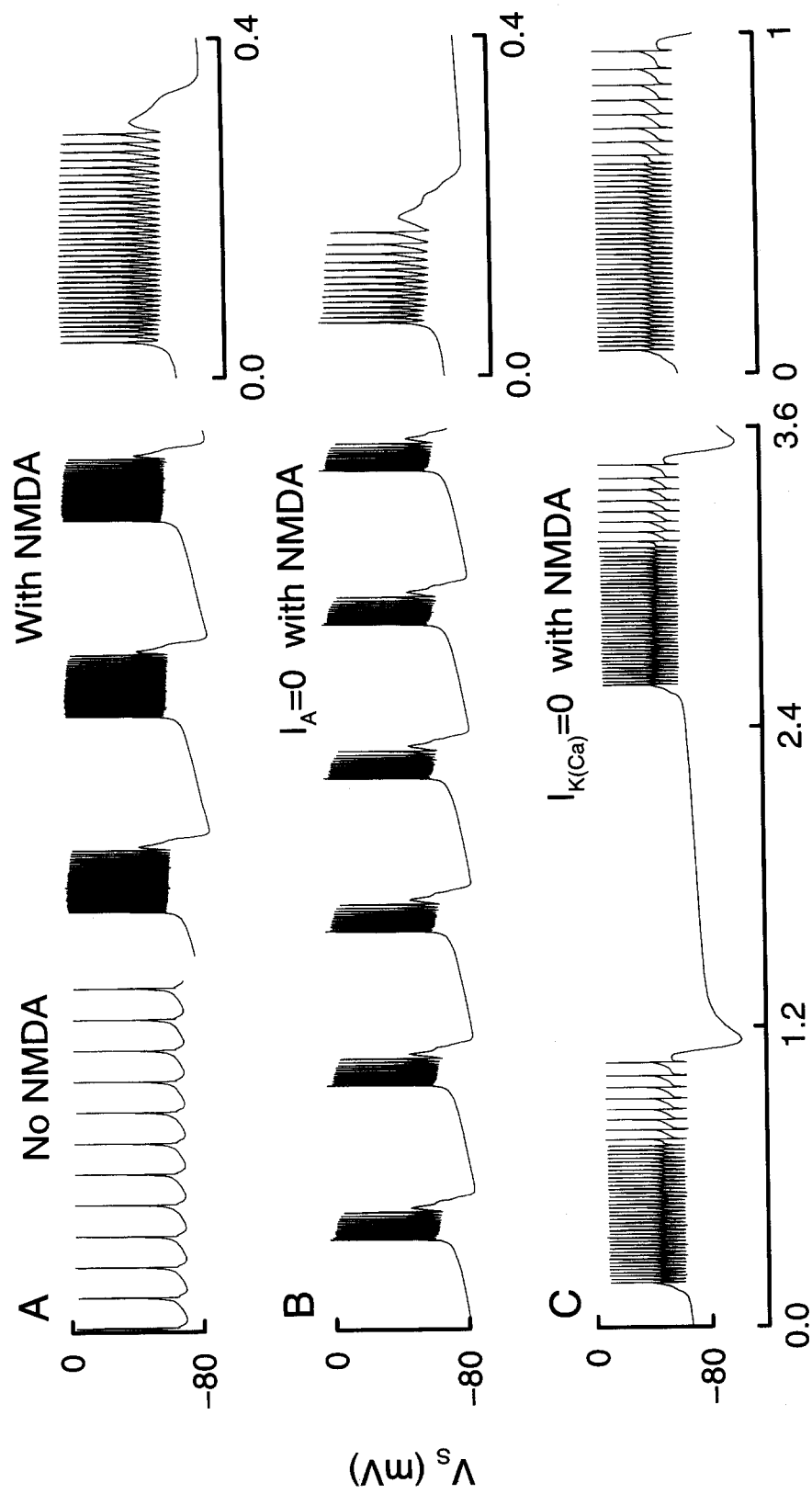

Fig. 6. NMDA-induced bursting profiles and frequency-adaptation in the more elaborate model of DA neurons. (A) Tonic spiking (~8 Hz) in the absence of NMDA is transformed into burst firing when NMDA is applied. (B) Frequency-adaptation in the absence of I_A when $I_{K(Ca)}$ is present. (C) A novel type of frequency-reduction, characterized by a sudden decrease of the spiking frequency during a burst, can occur in the absence of $I_{K(Ca)}$. The right panel of each row is an enlargement of one single spiking phase of the corresponding bursting pattern. As compared to the minimal model (see Fig. 3), the more elaborate model has bursting profiles that agree better with those observed in DA neurons. Parameter values used are (in mS/cm^2): $g_{K-DR,S} = 6.4$ in all panels $g_{K(Ca)} = 1.2$, $g_A = 2$ in A; $g_{K(Ca)} = 3.6$, $g_A = 0$ in B; and $g_{K(Ca)} = 0$, $g_A = 25$ in C. Other parameter values are taken from Table 1 (Appendix).

to the activation of NMDA or other glutamate receptors, but are intrinsic to the DA neuron model with its specific structure and channel composition.

In the minimal model presented above, the voltage spikes (Fig. 3A) are Na^+ action potentials generated by I_{Na} and $I_{K-DR,S}$. In the more elaborate model, however, voltage spikes can be generated in different ways. The very brief action potential spikes (Fig. 6A, left) are also Na^+ spikes mostly due to I_{Na} and $I_{K-DR,S}$, although other currents such as I_{Ca-T}, $I_{K(Ca)}$, I_A and I_h are also involved. Figure 7A shows that, when both I_{Na} and $I_{K-DR,S}$ are blocked, a different kind of voltage spike occurs. These spikes are broad ($\sim$50 ms duration), have a very small amplitude ($\sim$25 mV) and a lower frequency ($\sim$4 Hz) as compared to the Na^+ spikes in Fig. 6A ($\sim$9 Hz). Figure 7B demonstrates that these broad spikes persist when I_A and I_h are also eliminated, retaining a similar frequency and broadness but showing a large change in amplitude and profile. This shows that these broad spikes are actually Ca^{2+} action potentials produced by I_{Ca-T} and $I_{K(Ca)}$. In fact, similar Ca^{2+} action potential spikes have been observed experimentally in DA neurons[16,33] when I_{Na} and I_{K-DR} were blocked by TTX and TEA, respectively. Further computations demonstrate that the Ca^{2+} spikes plotted in Fig. 7B also persist in the soma when it is decoupled from the dendrite, indicating that the dendrite plays no role in the pacemaking of these Ca^{2+} spikes.

The low-threshold Ca^{2+} current I_{Ca-T} and the anomalous rectifier current I_h enable rebound excitation to occur when DA neurons are released from hyperpolarization.[16,23,28] This property is well characterized by the model (Fig. 7C). Simulations shown in Fig. 7C also suggest that under appropriate conditions, sustained injection of a moderate

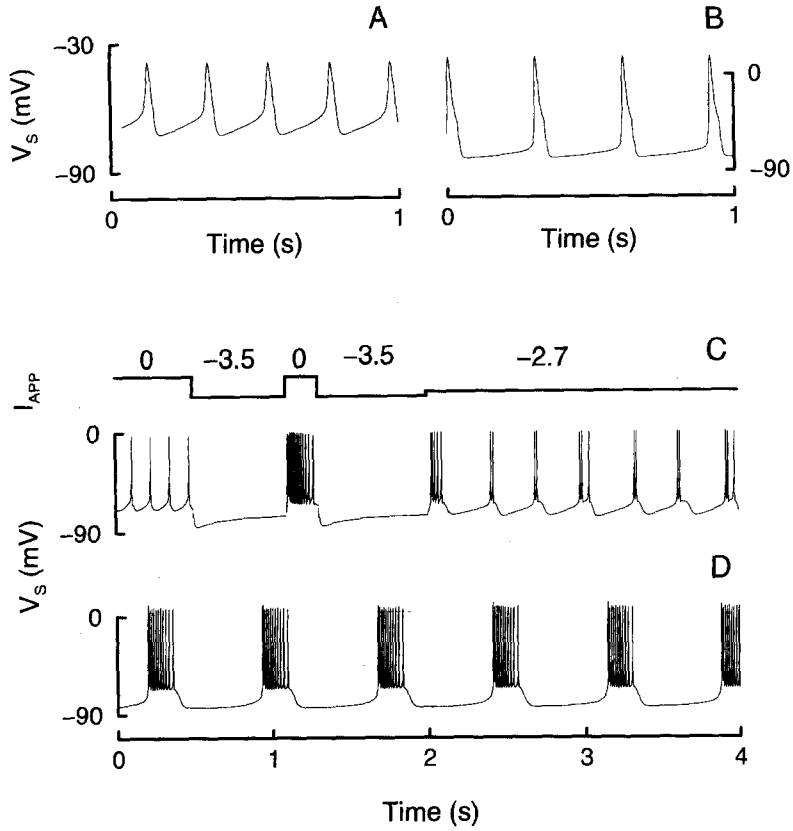

Fig. 7. Additional spiking and bursting patterns in the absence of NMDA. In A, broad Ca^{2+} action potentials occur when $I_{Na,S}$ and $I_{K-DR,S}$ are eliminated (i.e. $g_{Na,S} = g_{K-DR,S} = 0$). In B, these Ca^{2+} action potentials persist in the absence of I_A and I_h (i.e. $g_A = g_h = 0$). These broad voltage spikes also persist when the soma is disconnected from the dendrite (not shown). In both A and B, the tonic spiking state coexists with a depolarized stationary state at $V_S = V_D \approx 14$ mV. Therefore, those Ca^{2+} spikes can only be obtained when appropriate initial conditions are used (e.g., starting with the tonic spiking state in the presence of $I_{Na,S}$ and $I_{K-DR,S}$). Plotted in C are the computed responses of the model neuron to hyperpolarizing I_{APP} (in $\mu A/cm^2$) of different strength and duration. When $I_{APP} = -3.5$, tonic spiking is eliminated and V_S is hyperpolarized to about -80 mV. When released from this hyperpolarization, a rebound burst of action potentials occurs. When I_{APP} is moderate and sustained, a bursting pattern that differs from the NMDA-induced one is obtained. Such a bursting pattern can occur in the absence of I_A and I_h and when the soma is decoupled from the dendrite (D). Parameter values in A and B are from Table 1 (Appendix) except that in B, $g_{Ca-T} = 2.5$ (mS/cm^2). Those used in C and D are the same in Fig. 6A, except that $g_{NMDA} = g_{Na,NMDA} = 0$ and that $g_A = g_h = g_c = 0$ in D.

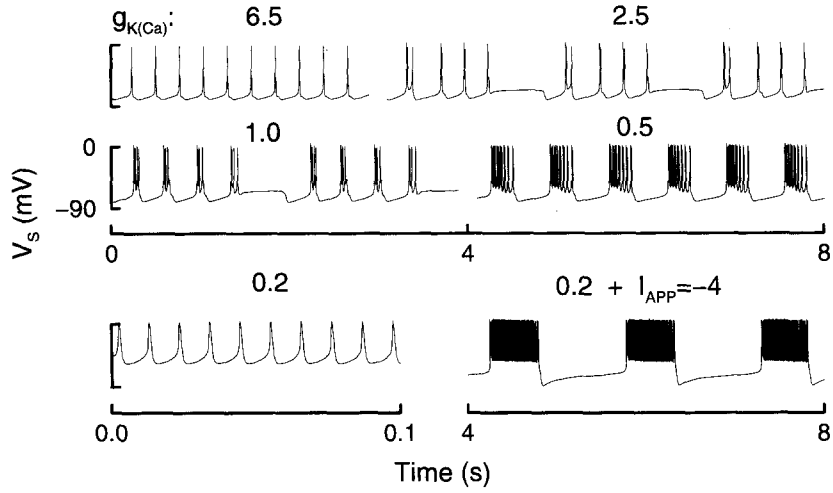

Fig. 8. The role of $I_{K(Ca)}$ in bursting of DA neurons in the presence of NMDA predicted by model computations. Successive decrease of the $I_{K(Ca)}$ conductance ($g_{K(Ca)}$ in mS/cm^2) from a value of 6.5 to 0.5 causes the transition from tonic spiking (left in the top panel) to episodic bursting (right in the top panel and left in the middle panel), and eventually causes the emergence of NMDA-induced regular bursting (right in middle panel). When $g_{K(Ca)}$ is negligibly small, the soma's excessive depolarization leads to very high frequency firing (~90 Hz, left in the bottom panel), which eliminates the NMDA-induced rhythmogenic capability of the dendritic compartment. However, when a hyperpolarizing current ($I_{APP} = -4\,\mu$A/cm^2) is injected to reduce the soma depolarization, NMDA-induced bursting reappears (right in the bottom panel). Parameter values are taken from Table 1 (Appendix), except that (in mS/cm^2): $g_{Ca-T} = 2.5$ and $g_{K-DR.D} = 2.4$.

hyperpolarizing current can cause burst firing in DA neurons that differs from the bursting induced by NMDA (a result yet to be tested). To reveal the essential elements underlying this bursting, I_A and I_h are eliminated from the soma compartment and the dendrite is decoupled in the simulation presented in Fig. 7D. This result indicates that I_{Ca-T} and $I_{K(Ca)}$ are the major contributors to this type of bursting. The slow time-scale is determined by Ca^{2+} accumulation in the soma compartment. Actually, $I_{K(Ca)}$ and slow Ca^{2+} handling have been studied extensively as a burst generating mechanism in previous models for other excitable cells and neurons.[6,35] It would be interesting to test whether this mechanism underlies the cesium-induced burst firing recently observed by Mercuri and co-workers[33] in DA neurons. Like the bursting shown in Fig. 7C and D, the cesium-induced bursting is also Ca^{2+}-dependent (i.e. it disappears in zero-Ca^{2+} medium).[33]

The role of $I_{K(Ca)}$ in N-*methyl*-D-*aspartate-induced bursting*. The involvement of $I_{K(Ca)}$ in burst-generation has been established in a number of neuron and endocrine cell types.[17,24,29,44] However, recent experiments on DA neurons have suggested a different role for $I_{K(Ca)}$ in burst generation, i.e. burst firing in the presence of NMDA is more easily observed when $I_{K(Ca)}$ is blocked by apamin.[26,40,41,42] Having shown that $I_{K(Ca)}$ plays a major role in generating broad calcium action potentials and a different bursting pattern associated with the slow Ca^{2+} accumulation in the soma compartment of the more elaborate model, we now explore how the $I_{K(Ca)}$-mediated bursting mechanism interacts with the NMDA-dependent bursting mechanism.

Figure 8 illustrates the role of $I_{K(Ca)}$ in burst firing of DA neurons in the presence of NMDA. Starting with a high value of $g_{K(Ca)}$ (left in the top panel), single spike firing (instead of bursting) occurs although the NMDA channel in the dendritic compartment is constantly activated. At lower values of $g_{K(Ca)}$ (right in the top panel and left in the middle panel) episodes of burst firing occur periodically; an episode's final burst gives way to a plateau. When $g_{K(Ca)}$ is further reduced, a regular bursting pattern emerges (right in the middle panel). This emergence of regular bursting at reduced $I_{K(Ca)}$ agrees with the rather surprising experimental observation[40,42] that reducing $I_{K(Ca)}$ enhances the occurrence of bursting in DA neurons. At negligible values of $g_{K(Ca)}$ (left in the bottom panel), the soma becomes very depolarized and fires action potentials with high frequency (~90 Hz) and high baseline (~ −60 mV) that eliminate the dendrite's capability to generate the NMDA-induced slow rhythm. However, if this somatic depolarization is depressed by an applied hyperpolarizing current, the NMDA-induced bursting reappears (right in the bottom panel). This seems to explain why an applied hyperpolarizing current was always needed when NMDA-induced bursting was recorded in the presence of apamin.[26,40,41]

The episodic bursting patterns reflect the interaction between two periodic, slow processes. The slowest one determines the repeat period of episodes (and the intervening long quiescent phase) while the

less slow one controls the bursting frequency during an episode. The faster one originates in the soma and is mainly due to the periodic activation of $I_{K(Ca)}$ by the elevated intrasoma Ca^{2+} concentration accumulated during each burst. This can be demonstrated by the persistence of these bursts of spikes when the soma and the dendrite are decoupled (result not shown). The longer time-scale periodicity, that determines the alternation between bursting and quiescence, is generated in the dendritic compartment and is due to the interaction between the NMDA channel and the Na^+ pump. This can be illustrated by computations of the model under the same conditions as those in Fig. 8 but with fixed intrasoma Ca^{2+} concentration. In such a case, the episodic bursting pattern is replaced by a normal NMDA-induced bursting pattern resembling that in the lower right panel of Fig. 8 (result not shown).

DISCUSSION

We have presented a two-compartment model of DA neurons of the basal ganglia, with special emphasis on the novel burst-generating mechanism of the NMDA channel/receptor interacting with the Na^+ pump in the distal dendrites. Burst firing generally involves two distinct processes that operate on significantly different time-scales: fast spiking and the slow alternation between spiking and quiescence.[2,37] The DA neuron of the substantia nigra is not unique in possessing a rich variety of channel types and multiple spike generating mechanisms.[16,23,28] Among the possible firing behaviors that can arise from mixing currents from this collection, a number of plausible burst generating mechanisms have been modeled and analysed in different contexts.[6,35,38] However, the slow wave of bursting in NMDA-bathed DA neurons in slice preparations appears to be due to a quite different mechanism, mediated by a pump current and a synaptic current without involving any intrinsic voltage-dependent channels. This unusual mechanism is mathematically formulated and explored here with a minimal, two compartment model. Our study confirms the viability of the NMDA-induced bursting mechanism recently proposed by Johnson and co-workers.[26]

We elaborated our minimal model to generate a more realistic NMDA-induced bursting profile, to account for several well established firing features, and to reveal additional spike and burst generating mechanisms in DA neurons. In exploring the unusual role of $I_{K(Ca)}$ in burst generation in DA neurons with this model, we reveal that, under certain conditions, large $I_{K(Ca)}$ can indeed eliminate NMDA-induced bursting, which only occurs when $I_{K(Ca)}$ is small (Fig. 8). However, when $I_{K(Ca)}$ is eliminated completely, NMDA-induced bursting also disappears because of the unopposed depolarization of the soma. In this case, a hyperpolarizing current injection can restore the NMDA-induced bursting (Fig. 8). These results agree well with experimental observations.[26,40–42] In particular, the model predicts (yet to be observed in experiments) the possible occurrence of some other complex firing modes, such as episodic bursting in DA neurons and complex transitions between different spiking modes (Fig. 8). It also predicts that $I_{K(Ca)}$-mediated, Ca^{2+}-dependent burst firing can occur in DA neurons (Fig. 7C, D). Further experiments of the type performed by Mercuri and co-workers[33] could help to test this prediction. For example, we expect that in the presence of apamin the bursts that they observed would be eliminated.

Burst firing resulting from NMDA channel activity has been observed in other neuron types including cat neocortical neurons,[11] motoneurons of the lamprey spinal cord,[43] rat abducens motoneurons,[9] and rat supraoptic nucleus neurons.[24] NMDA-induced bursting in these neurons and in apamin-bathed DA neurons share several important features: (i) it cannot be induced by somatic current injection in the absence of NMDA nor by non-NMDA agonists of glutamate; (ii) the slow rhythm underlying the burst firing persists with TTX application; and (iii) extracellular Mg^{2+}, which underlies the NMDA channel's voltage-sensitivity, is required to produce the slow rhythm. These features suggest that the NMDA channel is the crucial regenerative element. However, different mechanisms for producing the interburst hyperpolarization have been suggested for the neurons mentioned above. The increased $I_{K(Ca)}$ current resulting from Ca^{2+} entry through NMDA channels is believed to cause the interburst hyperpolarization in lamprey motoneurons[17] and rat supraoptic nuclei.[24] But in DA neurons[26] and in cat neocortical neurons[11] the slow rhythm persists in Ca^{2+}-free medium, thus excluding a major role for $I_{K(Ca)}$. Moreover, apamin, the $I_{K(Ca)}$-inhibitor, increases the chance of observing NMDA-induced bursting in DA neurons.[40] Our model results suggest that such a mechanism can generate NMDA-induced burst firing under some circumstances.

Early in our study, we explored the validity of the NMDA-induced bursting mechanism in a single-compartment model. We found that bursting occurs only when two seemingly implausible assumptions are made: (i) the pump and the NMDA channel are co-localized so that the pump senses only the domain Na^+ concentration at the mouth of an NMDA channel; (ii) the time-scale for pump activation by Na^+ is on the order of a second. The first assumption is needed so that the pump activation is sufficient to terminate spiking only when NMDA channels are open, while Na^+ entry through TTX-sensitive channels exerts little influence on pump activity. Since domains of high Na^+ concentration form and disappear with a fast time-scale, the second assumption introduces the slow time-scale required for generating the slow rhythm underlying the burst. In a previous model of NMDA-induced bursting in lamprey motor neurons, Brodin and colleages[4] encountered a similar problem. In order to segregate the Ca^{2+}-entry

through NMDA channels from that through voltage-gated Ca^{2+} channels, they assumed that Ca^{2+} through these pathways accumulates in two distinct cytoplasmic Ca^{2+} pools. By constructing a two-compartment model, we showed that segregated Na^{2+} handling arises naturally from cable-like compartmentalization of different Na^+ fluxes and that none of the special assumptions are needed. Moreover, a dendritic origin for the burst's slow wave, as in our two-compartment model, is consistent with recent observations of slow current oscillations when the soma is voltage-clamped at -60 mV.[41] Two- or three-compartment representations have also been shown necessary to model burst firing in CA3 neurons,[34] bursting in thalamic neurons,[7] and bistability in the firing patterns of motoneurons.[3]

Dopaminergic neurons in substantia nigra of the basal ganglia are involved in the control of affect, movement, and reward responses.[27,39] They project topographically to the striatum which receives extensive cortical and thalamic input, and which feeds back to the substantia nigra directly and indirectly through the globus pallidus and subthalamic nucleus. Efferents from the globus pallidus and substantia nigra extend to the thalamus, which in turn projects to the premotor and prefrontal cortex.[27] These connections constitute multiple loops of mutual feedback actions. The time-course of dopamine secretion onto the circuit elements in this system may be expected to modulate the activity. The functional significance of the burst firing pattern has been suggested by experiments showing that burst of spikes separated by quiescent periods were more potent in releasing dopamine than regularly spaced ones with the same average frequency.[13] A similar relationship was reported in hypothalamic magnocellular neurons.[10,36] In crayfish motoneurons, higher efficiency in triggering muscle response was associated with the bursting mode.[12] Therefore, the ability to generate several different firing modes is of great significance for a neuron to fulfill multiple functional requirements. Switching from tonic spiking to bursting through the activation of postsynaptic NMDA channels, a mechanism well established in several neuron types,[9,11,24,26,43] may prove to be an important *in vivo* mechanism of changing the firing mode of a neuron.

CONCLUSIONS

(1) Our mathematical model confirms the viability of a novel burst-generating mechanism[26] involving the interaction between the NMDA channel and an electrogenic Na^+ pump in distal dendrites. (2) The modeling indicates that the NMDA-mediated burst generating mechanism should be spatially segregated from the Na^+ influx through spike generating Na^+ channels, a conclusion that agrees well with recent experiments.[41] (3) Our more elaborate two-compartment model, with a soma compartment that encompasses the proximal dendrites and a dendritic compartment that lumps all distal dendrites, incorporates a plausible scheme of ion channel distribution in DA neurons suggested by experiments.[31] It represents a satisfactory, first-step model of DA neurons that is capable of reproducing several well established firing features of DA neurons. (4) The model clearly demonstrates the specific influence of $I_{K(Ca)}$ on NMDA-induced bursting in DA neurons. It also provides a plausible explanation for the necessity of a hyperpolarizing current injection for revealing the NMDA-induced bursting in the absence of $I_{K(Ca)}$. (5) The model predicts several other possible bursting modes, yet to be tested in DA neurons, including burst firing in the absence of NMDA that is mediated by $I_{K(Ca)}$ in the soma compartment.

REFERENCES

1. Asher P. and Nowak L. (1988) The role of divalent cations in the *N*-methyl-D-aspartate responses of mouse central neurons in culture. *J. Physiol., Lond.* **399,** 247–266.
2. Bertram R., Butte M. J., Kiemel T. and Sherman A. (1995) Topological and phenomenological classification of bursting oscillations. *Bull. Math. Biol.* **57,** 413–439.
3. Booth V. and Rinzel J. (1995) A minimal, compartmental model for a dendritic origin of bistability of motoneuron firing patterns. *J. Comput. Neurosci.* (in press).
4. Brodin L., Traven H. G. C., Lansner A., Wallen P., Ekeberg O. and Grillner S. (1991) Computer simulations of *N*-methyl-D-aspartate receptor-induced membrane properties in a neuron model. *J. Neurophysiol.* **66,** 473–484.
5. Cardozo D. L. (1993) Midbrain dopaminergic neurons from postnatal rat in long-term primary culture. *Neuroscience* **56,** 409–421.
6. Chay T. and Keizer J. (1983) Minimal model for membrane oscillations in the pancreatic β-cell. *Biophys. J.* **42,** 181–190.
7. Destexhe A., Contreras D., Steriade M., Sejnowski T. J. and Huguenard J. R. (1995) *In vivo, in vitro* and computational analysis of dendritic calcium currents in thalamic reticular neurons. *J. Neurosci.* (submitted).
8. De Weer P., Gadsby D. C. and Rakowski R. F. (1988) Voltage-dependence of the Na^+–K^+ pump. *A. Rev. Physiol.* **50,** 225–241.
9. Durand J. (1991) NMDA actions on rat abducens motoneurons. *Eur. J. Neurosci.* **3,** 621–633.
10. Dutton A. and Dyball R. E. J. (1979) Phasic firing enhances vasopressin release from the rat neurohypophysis. *J. Physiol., Lond.* **290,** 433–440.
11. Flatman J. A., Schwindt P. C., Crill W. E. and Stafstrom C. E. (1983) Multiple actions of *N*-methyl-D-aspartate on cat neocrotical neurons *in vitro*. *Brain Res.* **266,** 169–173.
12. Gillary H. L. and Kennedy D. (1969) Neuromuscular effects of impulse pattern in a crustacean motoneuron. *J. Neurophysiol.* **32,** 607–612.

13. Gonon F. G. (1988) Nonlinear relationship between impulse flow and dopamine release by rat midbrain dopaminergic neurons as studied by *in vivo* electrochemistry. *Neuroscience* **24,** 19–28.
14. Grace A. A. and Bunney B. S. (1984) The control of firing pattern in nigral dopamine neurons: single spike firing. *J. Neurosci.* **4,** 2866–2876.
15. Grace A. A. and Bunney B. S. (1984) The control of firing pattern in nigral dopamine neurons: burst firing. *J. Neurosci.* **4,** 2877–2890.
16. Grace A. A. and Onn S.-P. (1989) Morphology and electrophysiological properties of immunocytochemically identified rat dopamine neurons recorded *in vitro*. *J. Neurosci.* **9,** 3463–3481.
17. Grillner S. and Wallen P. (1985) The ionic mechanisms underlying *N*-methyl-D-aspartate receptor-induced, tetrodotoxin-resistant membrane potential oscillations in lamprey neurons active during locomotion. *Neurosci. Lett.* **60,** 289–294.
18. Hainsworth A. H., Roper J., Kapoor R. and Ashcroft F. M. (1991) Identification and electrophysiology of isolated pars compacta neurons from guinea-pig substantia nigra. *Neuroscience* **43,** 81–93.
19. Hilgemann D. W. (1994) Channel-like function of the Na,K pump probed at microsecond resolution in giant membrane patches. *Science, Washington, D.C.* **263,** 1429–1432.
20. Hindmarsh A. (1974) *An Ordinary Differential Equation Solver*. Report UCID-30001, Lawrence Livermore Laboratory.
21. Hodgkin A. L. and Huxley A. F. (1952) A quantitative description of membrane current and its application to conduction and excitation in nerve. *J. Physiol.*, **117,** 500–544.
22. Holmes W. R. and Levy W. B. (1990) Insights into associated long-term potentiation from computational models of NMDA receptor-mediated calcium influx and intracellular calcium concentration changes. *J. Neurophysiol.* **63,** 1148–1168.
23. Hounsgaard J., Nedergaard S. and Greenfield S. A. (1992) Electrophysiological localization of distinct calcium potentials at selective somatodendritic sites in the substantia nigra. *Neuroscience* **50,** 513–518.
24. Hu B. and Bourque C. W. (1992) NMDA receptor-mediated rhythmic bursting activity in rat supraoptic nucleus neurons *in vitro*. *J. Physiol., Lond.* **458,** 667–687.
25. Jahr C. E. and Stevens C. F. (1990) Voltage dependence of NMDA-activated macroscopic conductances predicted by single-channel kinetics. *J. Neurosci.* **10,** 3178–3182.
26. Johnson S. W., Seutin V. and North A. (1992) Burst firing in dopamine neurons induced by *N*-methyl-D-aspartate: role of electrogenic sodium pump. *Science, Washington, D.C.* **258,** 665–667.
27. Kandel E. R., Schwartz J. H. and Jessell T. M. (1991) *Principles of Neural Science*, 3rd edn, pp. 538–659. Elsevier, New York.
28. Kita T., Kita H. and Kitai S. T. (1986) Electric membrane properties of substantia nigra compacta neurons in an *in vitro* slice preparation. *Brain Res.* **372,** 21–30.
29. Kukuljan M., Stojilković S. S., Rojas E. and Catt K. J. (1992) Apamin-sensitive potassium channels mediate agonist-induced oscillations of membrane potential in pituitary gonadotrophs. *Fedn Eur. biochem. Socs Lett.* **301,** 19–22.
30. Li Y.-X., Bertram R. and Rinzel J. (1994) Modeling NMDA-induced bursting in dopamine neurons. *Soci. Neurosci. Abstr.* **20,** 1507.
31. Llinás R., Greenfield A. and Jahnsen H. (1984) Electrophysiology of pars compacta cells in the *in vitro* substantia nigra—a possible mechanism for dendritic release. *Brain Res.* **294,** 127–132.
32. Mayer M. L. and Westbrook G. L. (1985) The action of *N*-methyl-D-aspartatic acid on mouse spinal neurons in culture. *J. Physiol., Lond.* **361,** 65–90.
33. Mercuri N. B., Bonci A., Calabresi P., Stratta F., Stefani A. and Bernardi G. (1994) Effects of dihydropyridine calcium antagonists on rat midbrain dopaminergic neurones. *Br. J. Pharmac.* **113,** 831–838.
34. Pinsky P. and Rinzel J. (1994) Intrinsic and network rhythmogenesis in a reduced Traub model for CA3 neurons. *J. Comput. Neurosci.* **1,** 39–60.
35. Plant R. E. and Kim M. (1976) Mathematical description of a bursting pacemaker neuron by modification of the Hodgkin–Huxley equations. *Biophys. J.* **16,** 227–244.
36. Poulain D. A. and Wakerley J. B. (1982) Electrophysiology of hypothalamic magnocellular neurons secreting oxytocin and vasopressin. *Neuroscience* **7,** 773–808.
37. Rinzel J. (1987) A formal classification of bursting mechanisms in excitable systems. In *Mathematical Topics in Population Biology, Morphogenesis and Neurosciences* (eds Teramoto E. and Yamaguti M.), *Lect. Notes Biomath.* **71,** 267–281. Springer, Berlin.
38. Rush M. E. and Rinzel J. (1994) Analysis of bursting in a thalamic neuron model. *Biol. Cybern.* **71,** 281–291.
39. Schultz W., Apicella P., Ljungberg T., Romo R. and Scarnati E. (1993) Reward-related activity in monkey striatum and substantia nigra. *Prog. Brain Res.* **99,** 227–235.
40. Seutin V., Johnson S. W. and North A. (1993) Apamin increases NMDA-induced burst firing of rat mesencephalic dopamine neurons. *Brain Res.* **630,** 341–344.
41. Seutin V., Johnson S. W. and North A. (1994) Effect of dopamine and baclofen on NMDA-induced burst firing in rat ventral tegmental neurons. *Neuroscience* **58,** 201–206.
42. Shepard P. D. and Buney B. S. (1991) Repetitive firing properties of putative dopamine-containing neurons *in vitro*: regulation by an apamin-sensitive Ca^{2+}-activated K^+ conductance. *Expl Brain Res.* **86,** 141–150.
43. Sigvardt K. A., Grillner S., Wallen P. and Van Dongen P. A. M. (1985) Activation of NMDA receptors elicits fictive locomotion and bistable membrane properties in the lamprey spinal cord. *Brain Res.* **336,** 390–395.
44. Tse A. and Hille B. (1992) GnRH-induced Ca^{2+} oscillations and rhythmic hyperpolarizations of pituitary gonadotropes. *Science, Washington, D.C.* **255,** 462–464.

(*Accepted* 17 *October* 1995)

APPENDIX: A MORE ELABORATE MODEL: EQUATIONS AND PARAMETERS

We expand our minimal model incorporating additional ionic currents known to exist in DA neurons. However, we do not incorporate additional compartments into the two compartment structure of our model. According to a plausible

scheme of channel distribution in DA neurons proposed by Llinás and colleagues,[31] we put channels located in the soma and the proximal dendrites into our soma compartment, and include channels found in the distal dendrites in our dendritic compartment. Equations governing this improved model are given in Eqns 5–9:

$$C_m \frac{dV_S}{dt} = I_{APP} - I_{Na,S} - I_{Ca-T} - I_{K-DR,S} - I_{K(Ca)} - I_A - I_h - \frac{g_c}{p}(V_S - V_D), \quad \text{(Eqn 5)}$$

$$C_m \frac{dV_D}{dt} = -I_{Ca-L} - I_{K-DR,D} - I_{NMDA} - I_{pump} - I_L - \frac{g_c}{1-p}(V_D - V_S), \quad \text{(Eqn 6)}$$

$$\frac{dNa}{dt} = \alpha[-I_{Na,NMDA} - 3I_{pump}], \quad \text{(Eqn 7)}$$

$$\frac{dCa}{dt} = -\beta I_{Ca-T} - k_{Ca}Ca, \quad \text{(Eqn 8)}$$

$$\frac{dw}{dt} = [w_\infty - w]/\tau_w, \quad \text{(Eqn 9)}$$

where Ca denotes the Ca^{2+} concentration in the soma, Na represents the Na^+ concentration in the dendrite, w represents the 10 different gating variables. Na^+-handling in the soma and Ca^{2+}-handling in the dendrite are not considered in the model. The currents are defined as follows:

$$I_{Ca-T} = g_{Ca-T} m_T^2 h_T (V - V_{Ca}),\ I_{Ca-L} = g_{Ca-L} m_L^2 (V - V_{Ca}),$$

$$I_{K(Ca)} = g_{K(Ca)} (Ca^4/(Ca^4 + K_{Ca}^4))(V - V_K),$$

$$I_A = g_A a^4 b (V - V_K),\ I_h = g_h m_h (V - V_h);$$

$I_{Na,S}$ and $I_{K-DR,S}$ retain their definitions given in Eqn 1, while $I_{K-DR,D}$ assumes the same definition as $I_{K-DR,S}$, with V_S replaced by V_D. In Eqn 8, parameter β converts the Ca^{2+} current into Ca^{2+} flux, and k_{Ca} is the linear Ca^{2+} extrusion rate.

The steady-state activation/inactivation functions are defined as $m_\infty = 1/(1 + \exp(-(V_S + 35)/6.2))$, $h_\infty = 1/(1 + \exp[(V_S + 30)/8.3])$, $n_\infty = 1/(1 + \exp[-(V_S + 31)/5.3])$, $m_{T,\infty} = 1/(1 + \exp[-(V_S + 55)/7])$, $h_{T,\infty} = 1/(1 + \exp[(V_S + 81)/11])$, $a_\infty = 1/(1 + \exp[-(V_S + 60)/10])$, $b_\infty = 1/(1 + \exp[(V_S + 70)/5.7])$, and $m_{h,\infty} = 1/(1 + \exp[(V_S + 80)/8])$; $m_{L,\infty} = 1/(1 + \exp[-(V_D + 20)/5.3])$. The corresponding time constants are (in m): $\tau_h = 0.4[1 + 2/(1 + \exp[(V_S + 25)/5])]$, $\tau_n = 0.8[1 + 2/(1 + \exp[(V_S + 25)/10])]/(1 + \exp[-(V_S + 70)/10])$, $\tau_{m,T} = 1$, $\tau_{h,T} = 10$, $\tau_{m,L} = 0.4/[5\exp(\theta) + \theta/(\exp(\theta) - 1)]$ (with $\theta = -(V_D + 11)/8.3$), $\tau_a = 0.5$, $\tau_b = 10$, and $\tau_{m,h} = 190$.

The values of other parameters in our model are given in Table 1. We know of no voltage-clamp analysis and formulation of Hodgkin–Huxley-like expressions for the channel gating properties in DA neurons. Therefore, besides the "electrotonic" parameters (g_c and p) and the reversal potentials, most parameter values are taken from other neuron types possessing the same currents. The value of the maximum pump rate is chosen to best reproduce the observed firing patterns.

Table 1. Parameter values used in the model of dopamine neurons

Parameter	Model value	Parameter	Model value
C_m (specific capacitance)	$1\ \mu F/cm^2$	p	0.5
α	$0.173\ \frac{mM \cdot cm^2}{\mu A \cdot s}$	β	$0.104\ \frac{\mu M \cdot cm^2}{\mu A \cdot s}$
V_{Na}	55 mV	V_K	−85 mV
V_{Ca}	120 mV	V_h	−30 mV
V_L	−50 mV		
g_{NMDA}	$1.25\ mS/cm^2$	$g_{Na,NMDA}$	$1\ mS/cm^2$
$g_{Na,S}$	$3.2\ mS/cm^2$	$g_{K-DR,S}$	$3.2\ mS/cm^2$
g_A	$2\ mS/cm^2$	g_h	$0.1\ mS/cm^2$
g_{Ca-T}	$1.5\ mS/cm^2$	g_{Ca-L}	$0.19\ mS/cm^2$
$g_{K-DR,D}$	$0.14\ mS/cm^2$	g_L	$0.18\ mS/cm^2$
$g_{K(Ca)}$	$1.2\ mS/cm^2$	k_{Ca}	$1\ s^{-1}$
K_{Ca}	$0.4\ \mu M$	K_p	15 mM
R_{pump}	$18\ \mu A/cm^2$	N_{eq}	8 mM
$[Mg^{2+}]_o$	1.4 mM	K_{Mg}	10 mM
q	12.5 mV	g_c	$0.1\ mS/cm^2$